Research on a Tri-axial Differential-Drive In-Pipe Robot

Sheng-yuan Jiang[1,*], Xudong Jiang[1,2], Jie Lu[1], Jianyong Li[1], and Xiangyan Lv[1]

[1] College of Mechanical Engineering, Beihua University, Jilin 132021, China
[2] Institute of Mechanical Science and Engineering, Jilin University, Changchun 130022, China
Sheng-yuan Jiang, jiangshy_2002@163.com

Abstract. Pipelines for oil, gas and fluid transportation require a robot to have an excellent mobility and adaptability to various pipelines with elbows. In this paper, a novel differential drive in-pipe robot called tri-axial differential drive in-pipe robot, which is composed of a tri-axial differential mechanism and a pipeline adaptation mechanism, is presented and developed for the inspection of pipelines with inner diameter from 275 to 300 mm. The tri-axial differential mechanism with 3-DOF for steering allows the robot easily adapt to the existing configuration of pipelines by providing outstanding mobility during navigation. Then differential and mechanics property of the robot in straight pipeline and elbow are analyzed based on established mathematical model, and multi-body simulation on the robot is conducted to confirm the effectiveness of the proposed model.

Keywords: in-pipe robot, elbow, differential drive, tri-axial differential mechanism.

1 Introduction

In-pipe robots with intelligent navigating outfits have been developed for some inspection inside pipe such as corrosion, cracks and damage, and for operation tasks of coating and grinding. For space limited and complicated inner pipe environment, however, energy supply and environment adaptability are bottle-neck problems for long-distance navigation to in-pipe robots. Long-distance navigation demands in-pipe robots possessing outstanding performance such as environmental adaptability, large power to inertia ratio and large mobile velocity.

Now several in-pipe robots with steering capability have been reported, which are mainly classified into two groups, one is an articulated type and the other is a differential–drive one. The articulated type, usually composed of active articulated joints, drives the robot moving physically similar to the snake or the annelid animal in nature

* **Sheng-yuan Jiang** (1969-) received the Ph.D. degree from the Harbin Institute of Technology, Harbin, China, in 2001. Since 2002, he has been with Beihua University, Jilin, China, where he is currently a Professor in the college of Mechanical Engineering. He works on robotics, mainly on mechanism of the robot and special robot. Mobile phone: 0086-013944693103;0086-0432-5580001.

C. Xiong et al. (Eds.): ICIRA 2008, Part I, LNAI 5314, pp. 1031–1040, 2008.

[1], [2], [3]. As one of the most adequate mechanisms, steering mechanism of the articulated type becomes complicated, for example, steering joint [4], [5], [6], rubber gas-actuated joint [7], and double active universal joint [8], [9]. These robots can move along elbows.

As alternative approach, the differential–drive type performs steering by modulating the speeds of driving wheels based on prerequisite modeling and analysis on movements determined by pipeline configurations [10~15]. In these work, differential performance of the differential–drive type is mainly determined by systematical model and control algorithm.

2 Configuration and Mechanism of the Robot

As depicted in Fig.1 and 2, tri-axial differential drive in-pipe robot mainly consists of two parts, the driving module and the pressure modulating module. The radius covered by the robot, with axial constant length of 550 mm, varies from 275 to 300 mm, as illustrated in Fig.2. The traction force of the robot is 450 N, the maximum speed is 0.2 m/s and the own weight of the robot is 30 Kg.

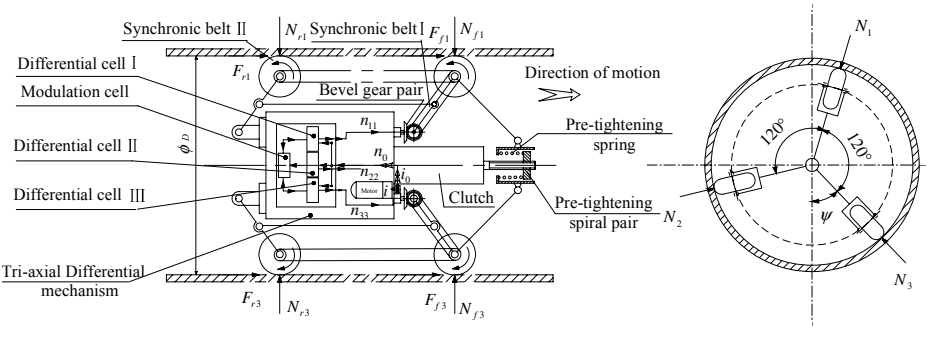

Fig. 1. Configuration principle of the robot

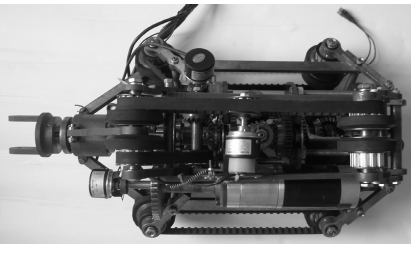

Fig. 2. Tri-axial differential-drive in-pipe robot

2.1 Driving Module

The driving module primarily consists of a geared DC motor (Maxon, 120 W) with an encoder, tri-axial differential mechanism and several bevel gears, as shown in Fig.3.

The front wheel is driven with a single motor via gear transmission, and the rear one is driven by the front counterpart via synchronic belt transition as shown in Fig. 1, where i_0 denotes the transmission ratio from the motor to tri-axial differential mechanism. Since the transition ratio of the synchronic belt Ⅰ, Ⅱ as well as the the bevel gears is identical to one, as shown in Fig.1, the rotation speed of the front wheel is the same as the corresponding output rotation speed of the tri-axial differential mechanism.

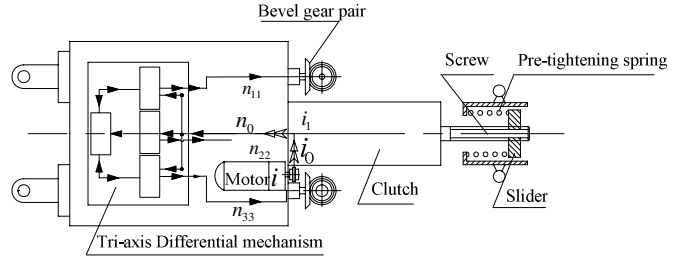

(a) Outline of the driving module

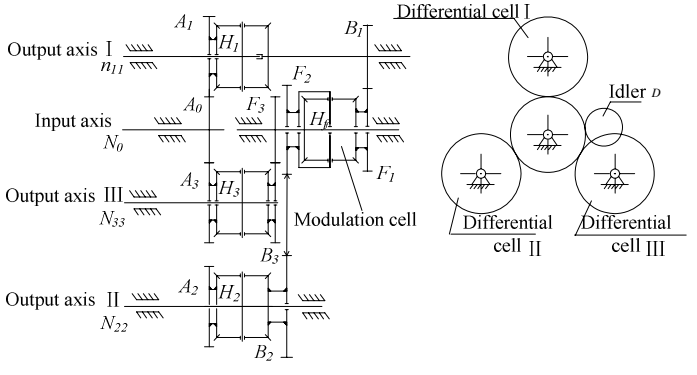

(b) Tri-axial differential mechanism

Fig. 3. The driving module

The tri-axial differential mechanism is a parallel 3-DOF mechanism with axial symmetry as depicted in Fig.3. The mechanism consists of four differential gear trains called differential cell- Ⅰ, Ⅱ,Ⅲ, and modulation cell respectively. When moving in the workspace such as straight and elbow pipe, the modulation cell of the mechanism modulates each differential cell to make the robot subjected to different geometry constraints and hence avoid slippage. In case of straight pipeline, since the speeds of the wheels should be the same as one another, the modulation cell does not operate and degenerate to be a fixed-axial gear train. In elbow, since the speeds of the wheels should be different from one another, the modulation cell modulates each differential cell to make the wheels avoid slippage. As a result of six active drive wheels, the

driving module amplifies traction forces, by supplying the robot with sufficient traction forces for moving inside various pipelines.

2.2 Pressure Modulating Module

As illustrated in Fig.1, the pressure modulating module is a skeletal linkage mechanism. It is composed one set of slider-crank mechanisms, which consists of three slider-crank mechanisms located equidistantly along the circumferential direction. Radial motions of wheels are synchronized with a slider illustrated in Fig.1 and 3(a), and its axial motion is limited by self-lock of spiral fit between slider and screw. The front wheels and the rear ones, called the front and rear wheel set, are allowed to move synchronically since each front wheel and its rear counterpart are connected with synchronic belt. In the proposed mechanism, the distance between the central axis and the wheel center is determined by the movement of the slider, enclosed by an elastic restoration force from a spring connected between the slider and the wall.

Since the proposed mechanism has been designed to make the wheels have effective contacts against the inner wall of pipelines to be suitable for diversified pipelines, the robot is adaptable to some indefinite pipeline conditions, as well as provision with sufficient traction forces during movements.

3 Differential Model of the Robot

Differential characteristics of the robot is analyzed both in the straight and elbow as follows. Assuming that a disk with negligible thickness is moving along the pipeline and its central rotating axis coincides with that of the pipeline. Then motion state of each wheel is determined after deriving differential equations of the robot.

As illustrated in Fig.4, an elbow with inner diameter of D is similar to a part of a torus. An absolute coordinate frame $O-(x, y, z)$ is attached to the center of the torus, where z -axis is along the axis of rotation axis of elbow, and the other two orthogonal axes, x-axis and y -axis are set along the radial directions. According to the regulation of urban oil supply equipment, curvature radius R should be 1.5 times larger than the inner diameter of elbow, i.e. $R = 3.5D$. The trajectory of contact point of each wheel is located in the pipeline with inner diameter D , whereas the center of each wheel with its diameter d in the "pipeline"with its inner diameter $D-d$. In the elbow, the speeds of the wheels should be different from one another, depending on the contact point against the wall of the pipelines, combined with the curvature of the wheel center. According to [16], the motion equation of each wheel of the robot can be written by

$$n_{11} + n_{22} + n_{33} = -1.5 i_0 n_0 \tag{1}$$

Where $n_{ii}(i = 1, 2, 3)$ represents the parameter of output rotational speed for the tri-axial differential mechanism identical to that of the front wheel set, n_0 denotes input rotational speed.

3.1 Differential Model of the Robot in Straight Pipeline

In straight pipe, the robot does not perform differential operation with the wheels purely rolling, and rotational speed of each wheel of the robot satisfies its corresponding constraint equation in straight pipeline, is determined by Eq. (1) and (2).

$$\begin{cases} v_{fi} = 0.5dn_{ii}, v_{ri} = 0.5dn_{ii} \\ \qquad (i = 1,2,3) \\ v_{f1} = v_{f2} = v_{f3} = v_{r1} = v_{r2} = v_{r3} \end{cases} \tag{2}$$

3.2 Differential Equations of the Robot in Elbow

As depicted in Fig.4, the projections Ⅰ - Ⅰ of the wheel centers at the front wheel set is the same as the projections Ⅱ - Ⅱ at the rear wheel set, since the robot is axial symmetrical, and the following equation can be derived

$$R_{fi} = R_{ri} \quad (i = 1,2,3) \tag{3}$$

$$v_{f1} : v_{f2} : v_{f3} = R_{f1} : R_{f2} : R_{f3} = n_{11} : n_{22} : n_{33} \tag{4}$$

$$v_{r1} : v_{r2} : v_{r3} = R_{r1} : R_{r2} : R_{r3} \tag{5}$$

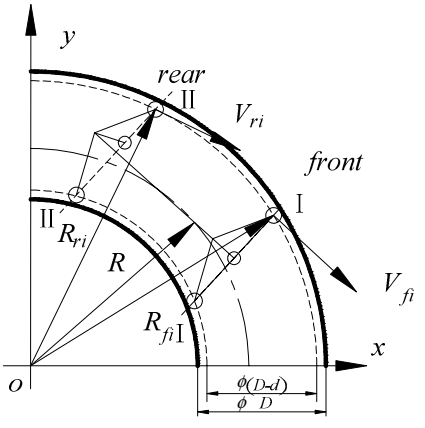

Fig. 4. Principle of differential velocity of the robot

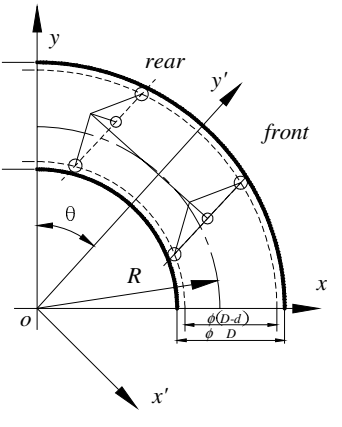

Fig. 5. Coordinate frame of the robot in elbow

where v_{fi}, R_{fi} represent velocity of the wheel centers and its curvature radius at the front wheel set respectively, while v_{ri}, R_{ri} at the rear wheel set respectively. Combined with equation (3) ~ (5), the velocity ratio of each wheel center can be written by

$$v_{f1} : v_{f2} : v_{f3} : v_{r1} : v_{r2} : v_{r3} = n_{11} : n_{22} : n_{33} : n_{11} : n_{22} : n_{33} \tag{6}$$

4 Moving Mechanics Model of the Robot

Based on mechanics equations of pipeline adaptation mechanism in elbow and straight pipeline by virtual displacement principle as discussed in previous section, mechanics equations of the robot are derived in latter section. The moving coordinate frames $O-(x', y', z')$ and $E-(x'', y'', z'')$ are attached to the robot for describing mechanics property of the robot and its pipeline adaptation mechanism respectively as depicted in Fig.5 and 6. According to [8~11], the mathematical expression of geometry elbow $\boldsymbol{W}(\phi,\lambda)\in R^3$ and straight pipeline can write by

$$\boldsymbol{W}(\phi,\lambda)=\left[(R+0.5D\mathrm{c}\phi)\mathrm{c}\lambda \quad (R+0.5D\mathrm{c}\phi)\mathrm{s}\lambda \quad 0.5D\mathrm{s}\phi\right]^{\mathrm{T}} \tag{7}$$

$$(y-R)^2+z^2=D^2/4 \tag{8}$$

where, the definition of parameter ϕ and λ are specified in [8~11]. By assuming that the parameters in body moving coordinate marked with superscript of apostrophe, the motion parameters of front and rear wheels marked with subscript of *f* and *r* respectively, the parameters related to wheel center marked with subscript of *c*.

4.1 Mechanics Model of the Adaptation Mechanism in Eelbow

As illustrated in Fig.5, according to geometry constraint in elbow and adaptation mechanism, the trajectory equations of the first front wheel center, the rear one and application point H of the spring (9) ~ (13) are derived and subsequently virtual displacement equation (14) ~ (19).

$$\boldsymbol{W}(\phi,\lambda,\alpha)=\boldsymbol{W}_{\mathrm{c}}(\phi,\lambda,\alpha)+0.5d\boldsymbol{n}(\phi,\lambda) \tag{9}$$

$$\boldsymbol{W}''_{\mathrm{fc1}}=\left[L_3\mathrm{c}\alpha \quad L_3\mathrm{s}\alpha \quad 0\right]^{\mathrm{T}} \tag{10}$$

$$\boldsymbol{W}''_{\mathrm{rc1}}=\left[-L+L_3\mathrm{c}\alpha \quad L_3\mathrm{s}\alpha \quad 0\right]^{\mathrm{T}} \tag{11}$$

$$\boldsymbol{H}=\left[L_3\mathrm{c}\alpha+L_4\mathrm{c}\beta \quad L_2-L_1 \quad 0\right]^{\mathrm{T}} \tag{12}$$

$$L_3\mathrm{s}\alpha+L_1=L_4\mathrm{s}\beta+L_2 \tag{13}$$

$$L_3\mathrm{c}\alpha\delta\alpha=L_4\mathrm{c}\beta\delta\beta \tag{14}$$

$$\delta\boldsymbol{W}''_{\mathrm{fc1}}=\left[-L_3\mathrm{s}\alpha\delta\alpha \quad L_3\mathrm{c}\alpha\delta\alpha \quad 0\right]^{\mathrm{T}} \tag{15}$$

$$\delta\boldsymbol{W}''_{\mathrm{rc1}}=\left[-L_3\mathrm{s}\alpha\delta\alpha \quad L_3\mathrm{c}\alpha\delta\alpha \quad 0\right]^{\mathrm{T}} \tag{16}$$

$$\delta\boldsymbol{H}=\left[-L_3\mathrm{s}\alpha\delta\alpha-L_3\mathrm{c}\alpha\left(L_3\mathrm{s}\alpha+L_1-L_2\right)\Big/\sqrt{L_4^2-\left(L_3\mathrm{s}\alpha+L_1-L_2\right)^2} \quad L_2-L_1 \quad 0\right]^{\mathrm{T}} \tag{17}$$

$$\delta \boldsymbol{W}_{\mathrm{fc1}}=\begin{bmatrix}\mathrm{c}\theta & -\mathrm{s}\theta & 0\\ \mathrm{s}\theta & \mathrm{c}\theta & 0\\ 0 & 0 & 1\end{bmatrix}\begin{bmatrix}1 & 0 & 0\\ 0 & \mathrm{c}\left(60^{\circ}-\psi\right) & -\mathrm{s}\left(60^{\circ}-\psi\right)\\ 0 & \mathrm{s}\left(60^{\circ}-\psi\right) & \mathrm{c}\left(60^{\circ}-\psi\right)\end{bmatrix}\begin{bmatrix}-L_3\mathrm{s}\alpha\delta\alpha\\ L_3\mathrm{c}\alpha\delta\alpha\\ 0\end{bmatrix} \tag{18}$$

$$\delta \boldsymbol{W}_{\mathrm{rc1}}=\begin{bmatrix}\mathrm{c}\theta & -\mathrm{s}\theta & 0\\ \mathrm{s}\theta & \mathrm{c}\theta & 0\\ 0 & 0 & 1\end{bmatrix}\begin{bmatrix}1 & 0 & 0\\ 0 & \mathrm{c}\left(60^{\circ}-\psi\right) & -\mathrm{s}\left(60^{\circ}-\psi\right)\\ 0 & \mathrm{s}\left(60^{\circ}-\psi\right) & \mathrm{c}\left(60^{\circ}-\psi\right)\end{bmatrix}\begin{bmatrix}-L_3\mathrm{s}\alpha\delta\alpha\\ L_3\mathrm{c}\alpha\delta\alpha\\ 0\end{bmatrix} \tag{19}$$

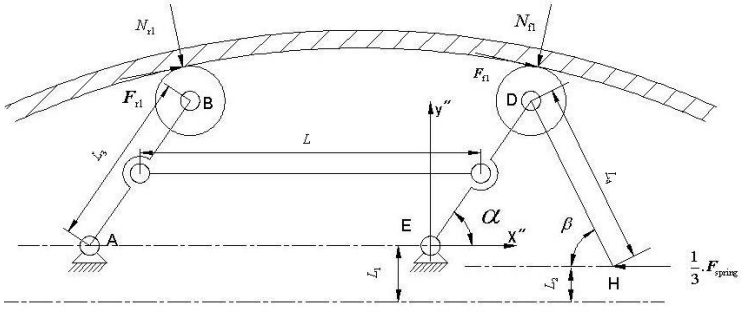

Fig. 6. Force analysis diagram for pipe diameter adaptation mechanism in elbow pipeline

The virtual displacement of other four wheel centers $\delta \boldsymbol{W}_{\mathrm{fc2}}$、$\delta \boldsymbol{W}_{\mathrm{fc3}}$、$\delta \boldsymbol{W}_{\mathrm{rc2}}$、$\delta \boldsymbol{W}_{\mathrm{rc3}}$ is derived in unified frame. According to (9), we have

$$\delta \boldsymbol{W}\left(\phi,\lambda,\alpha\right)=\delta \boldsymbol{W}_{\mathrm{c}}\left(\phi,\lambda,\alpha\right) \tag{20}$$

$$\delta \boldsymbol{W}_{\mathrm{f}i}\left(\phi,\lambda,\alpha\right)=\delta \boldsymbol{W}_{\mathrm{fc}i}\left(\phi,\lambda,\alpha\right)(i=1,2,3) \tag{21}$$

$$\delta \boldsymbol{W}_{\mathrm{r}i}\left(\phi,\lambda,\alpha\right)=\delta \boldsymbol{W}_{\mathrm{rc}i}\left(\phi,\lambda,\alpha\right)(i=1,2,3) \tag{22}$$

$$\boldsymbol{N}_{\mathrm{f}i}=N_{\mathrm{f}i}\boldsymbol{n}_{\mathrm{f}i}=N_{\mathrm{f}i}\begin{bmatrix}\mathrm{c}\phi_{\mathrm{f}i}\mathrm{c}\lambda_{\mathrm{f}i} & \mathrm{c}\phi_{\mathrm{f}i}\mathrm{s}\lambda_{\mathrm{f}i} & \mathrm{s}\phi_{\mathrm{f}i}\end{bmatrix}^{\mathrm{T}} \tag{23}$$

$$\boldsymbol{N}_{\mathrm{r}i}=N_{\mathrm{r}i}\boldsymbol{n}_{\mathrm{r}i}=N_{\mathrm{r}i}\begin{bmatrix}\mathrm{c}\phi_{\mathrm{r}i}\mathrm{c}\lambda_{\mathrm{r}i} & \mathrm{c}\phi_{\mathrm{r}i}\mathrm{s}\lambda_{\mathrm{r}i} & \mathrm{s}\phi_{\mathrm{r}i}\end{bmatrix}^{\mathrm{T}} \tag{24}$$

$$\boldsymbol{F}_{\mathrm{spring}}=\begin{bmatrix}-F_{\mathrm{spring}} & 0 & 0\end{bmatrix}^{\mathrm{T}} \tag{25}$$

Based on virtual displacement principle, virtual displacement equation of the pipeline adaptation mechanism is represented as

$$\sum_{i=1}^{3}\boldsymbol{N}_{\mathrm{f}i}\bullet\delta \boldsymbol{W}_{\mathrm{f}i}+\sum_{i=1}^{3}\boldsymbol{N}_{\mathrm{r}i}\bullet\delta \boldsymbol{W}_{\mathrm{r}i}+\boldsymbol{F}_{\mathrm{spring}}\bullet\delta \boldsymbol{H}=0 \tag{26}$$

Combined with (9) ~ (26), $\boldsymbol{F}_{\text{spring}}$, the spring force applied to adaptation mechanism is quantitatively determined by the location angle θ and posture angle ψ in elbow. In the case of straight pipeline, substituting $\theta = 0^\circ$, $\lambda_{\text{f}i} = \lambda_{\text{r}i} = 90^\circ$ to (26), and the simplified case in straight pipeline is obtained.

4.2 Mechanics Model of the Robot

According to (7) and (8), the unit normal vector and unit tangible vector in straight and those in elbow are represented respectively by

$$\begin{cases} \boldsymbol{n}_{\text{straight}} = \begin{bmatrix} 0 & \dfrac{y-R}{0.5D} & \dfrac{z}{0.5D} \end{bmatrix}^{\text{T}} \\ \boldsymbol{t}_{\text{straight}} = \begin{bmatrix} 1 & 0 & 0 \end{bmatrix}^{\text{T}} \end{cases} \tag{27}$$

$$\begin{cases} \boldsymbol{n}_{\text{elbow}} = \begin{bmatrix} \text{c}\phi\text{c}\lambda & \text{c}\phi\text{s}\lambda & \text{s}\phi \end{bmatrix}^{\text{T}} \\ \boldsymbol{t}_{\text{elbow}} = \begin{bmatrix} \text{s}\lambda & -\text{c}\lambda & 0 \end{bmatrix}^{\text{T}} \end{cases} \tag{28}$$

With the robot uniformly moving, the equilibrium equation are satisfied by

$$\sum \boldsymbol{F} = \sum_{i=1}^{3} \left(\boldsymbol{N}_{\text{f}i} + \boldsymbol{N}_{\text{r}i} + \boldsymbol{F}_{\text{f}i} + \boldsymbol{F}_{\text{r}i} \right) + \boldsymbol{G} = 0 \tag{29}$$

$$\begin{cases} \boldsymbol{N}_{\text{f}i} = N_{\text{f}i}\boldsymbol{n}_{\text{f}i} \\ \boldsymbol{N}_{\text{r}i} = N_{\text{r}i}\boldsymbol{n}_{\text{r}i} \end{cases} \quad (i = 1,2,3) \qquad \begin{cases} \boldsymbol{F}_{\text{f}i} = \mu N_{\text{f}i}\boldsymbol{t}_{\text{f}i} \\ \boldsymbol{F}_{\text{r}i} = \mu N_{\text{r}i}\boldsymbol{t}_{\text{r}i} \end{cases} \quad (i = 1,2,3) \tag{30}$$

$$\sum \boldsymbol{M} = \sum_{i=1}^{3} \left[\boldsymbol{W}_{\text{f}i} \times \left(\boldsymbol{N}_{\text{f}i} + \boldsymbol{F}_{\text{f}i} \right) + \boldsymbol{W}_{\text{r}i} \times \left(\boldsymbol{N}_{\text{r}i} + \boldsymbol{F}_{\text{r}i} \right) \right] + \boldsymbol{W}_{G} \times \boldsymbol{G} = 0 \tag{31}$$

where G represents the gravity of the robot, $\boldsymbol{n}_{\text{f}i}$, $\boldsymbol{t}_{\text{f}i}$ and $\boldsymbol{N}_{\text{f}i}$ denote the unit normal vector, the unit tangible vector and the normal pressure at the contact points of the front wheels against the wall, whereas $\boldsymbol{n}_{\text{r}i}$, $\boldsymbol{t}_{\text{r}i}$ and $\boldsymbol{N}_{\text{r}i}$ represent the counterparts of the rear wheels.

Combined with (28)~(31), the contact normal pressure and friction of the robot against the wall are derived to determine its moving mechanics model . Then the force applied to spring is calculated by Eq. (26).

5 Virtual Experiment on Mobility Property of the Robot

To confirm the effectiveness of above theoretical model, virtual test on the robot has been performed when the posure angle $\psi = 0^\circ$. The virtual prototype of the robot is modelled according to the prototyoe as shown in Fig.2.

The simulation curves illustrated that the differential property and mechanic property of the robot have been identified:

In straight pipeline, the rotation speed of each wheel is the same and hence the robot does not perform differential drive in consistence with theoretical model.

Either in straight pipeline or in elbow, since the velocity of front wheel set at wheel center is the same as the counterpart of the rear wheel set, each wheel purely roll without parasite power in coincidence with theoretical model.

Although there is weak contact at a wheel against the wall of pipeline in elbow, the front wheel set and rear wheel set are simultaneously drive to ensure sufficient traction forces.

In elbow, the radial compression of adaptation mechanism is actuated into function by geometry constraint.

6 Conclusion

A novel differential drive in-pipe robot composed of a tri-axial differential mechanism and a pipeline adaptation mechanism are designed for moving inside pipelines. Both differential model and mechanics model in straight and elbow pipes are analyzed theoretically. In straight pipe, the robot does not perform differential operation whereas in elbow pipe, it realizes autonomous differential operation with the wheels purely rolling by the geometry constraint of in-pipe environment and hence without parasite power. It is indicated that the robot has laid a foundation for theoretical research of differential in-pipe robot with good mechanical adaptability.

Acknowledgments

This work was supported in the National '863' plan, the People's Republic of China, under Contract No. 2006AA04Z236. This work is also supported by Program for New Century Excellent Talents in University in 2007, Ministry of Education, the People's Republic of China.

References

1. Granosik, G., Borenstein, J.: Integrated joint actuator for serpentine robots. IEEE/ASME Transaction on Mechatronics 10(5), 473–481 (2005)
2. Wakimoto, S., Nakajima, J., Takata, M., et al.: A micro snake-like robot for small pipe inspection. In: Proceedings of the IEEE International Symposium on Micromechatronics and Human Science, pp. 303–308. IEEE, Piscataway (2003)
3. Chen, L., Wang, Y.C., Ma, S.G., et al.: Analysis of traveling wave locomotion of snake robot. Chinese Journal of Mechanical Engineering 40(12), 38–43 (2003)
4. Scholl, K.U., Kepplin, V., Berns, K., Dillmann, R.: Controlling a multi-joint robot for autonomous sewer inspection. In: Proc. IEEE Int. Conf. Robotics, Automation, vol. 2, pp. 24–28 (2000)
5. Schempf, H., Vradis, G.: Explorer: Long-range untethered real-time live gas main inspection system. In: Proc. Conf. GTI, http://www.rec.ri.cmu.edu/projects/explorer

6. Gamble, B.B., Wiesman, R.M.: Tethered Mouse System for Inspection of Gas Distribution Mains. Gas Res. Inst., Doc., GRI-96/0209 (1996)
7. Fukuda, T., Hosokai, H., Uemura, M.: Rubber gas actuator driven by hydrogen storage alloy for in-pipe inspection mobile robot with flexible structure. In: Proc. IEEE Int. Conf. Robotics, Automation, vol. 3, pp. 1847–1852 (1989)
8. Choi, H., Ryew, S.: Robotic system with active steering capability for internal inspection of urban gas pipelines. Mechatronics 26(1), 105–112 (2002)
9. Ryew, S.M., Baik, S.H., Ryu, S.W., Jung, K.M., Roh, S.G., Choi, H.R.: Inpipe inspection robot system with active steering mechanism. In: Proc. IEEE Int. Conf. Intelligent Robots, Systems, pp. 1652–1657 (2000)
10. Roh, S.G., Ryew, S.M., Yang, J.H., et al.: Actively steerable in-pipe inspection robots for underground urban gas pipeline. In: Proceeding of the IEEE International Conference on Robotics and Automation, pp. 761–766. IEEE, Piscataway (2001)
11. Roh, S.G., Choi, H.R.: Differential-drive in-pipe robot for moving inside urban gas pipelines. IEEE Transactions on Robotics 21(1), 1–17 (2005)
12. Deng, Z.Q., Chen, J., Jiang, S.Y.: Traction robot drive by six independent wheels for inspection inside pipeline. Chinese Journal of Mechanical Engineering 41(9), 67–72 (2005)
13. Zhang, X.H., Chen, H.J.: Independent wheel drive and fuzzy control of mobile pipeline robot with vision. In: Proceedings of the Annual Conference of the IEEE Industrial Electronics Society, pp. 2526–2530. IEEE, Piscataway (2003)
14. Xu, F.P., Deng, Z.Q.: Research on traveling-capability of pipeline robot in elbow. Robot 26(2), 155–160 (2004)
15. Deng, Z.Q., Chen, J., Jiang, S.Y.: Development of in-pipe robot drived by six independent wheels. High Technology Letters 14(9), 54–58 (2004)